

DEAP-3600 - Latest results from the largest liquid argon dark matter experiment

Roxanne Turcotte-Tardif^{a,b,*} and the DEAP-3600 Collaboration[†]

^aDepartment of Physics, Carleton University, Ottawa, Ontario, K1S 5B6, Canada

^bArthur B. McDonald Canadian Astroparticle Research Institute, Queen's University, Kingston, Ontario, K7L 3N6, Canada

E-mail: roxanneturcotte@cunet.carleton.ca

DEAP-3600 is a multi-tonne experiment at SNOLAB, an underground laboratory located at a depth of 2 km in Sudbury, Canada. The detector is filled with approximately 3.3 tonnes of liquid argon contained in a 1.7 m diameter ultra-low-background acrylic vessel operating at a temperature of 87 K and is designed for the direct detection of Weakly Interacting Massive Particles (WIMPs), one of the most promising dark matter candidates. DEAP-3600 sets world-leading constraints on TeV-scale mass dark matter searches with liquid argon as scattering target, as well as on Planck-scale mass dark matter. The detector relies on the pulse shape discrimination method, which allows the rejection of electronic recoil backgrounds with better than 10^{-10} leakage probability at 50% nuclear recoil acceptance above 18 keVee. In this contribution, the latest results from DEAP-3600 will be presented, including a description of the background model as well as dark matter search results.

38th International Cosmic Ray Conference (ICRC2023)

26 July - 3 August, 2023

Nagoya, Japan



[†] We thank the Natural Sciences and Engineering Research Council of Canada (NSERC), the Canada Foundation for Innovation (CFI), the Ontario Ministry of Research and Innovation (MRI), and Alberta Advanced Education and Technology (ASRIP), the University of Alberta, Carleton University, Queen's University, the Canada First Research Excellence Fund through the Arthur B. McDonald Canadian Astroparticle Physics Research Institute, Consejo Nacional de Ciencia y Tecnología Project No. CONACYT CB-2017-2018/A1-S-8960, DGAPA UNAM Grants No. PAPIIT IN108020 and IN105923, and Fundación Marcos Moshinsky, the European Research Council Project (ERC StG 279980), the UK Science and Technology Facilities Council (STFC) (ST/K002570/1 and ST/R002908/1), the Leverhulme Trust (ECF-20130496), the Russian Science Foundation (Grant No. 21-72-10065), the Spanish Ministry of Science and Innovation (PID2019-109374GB-I00) and the Community of Madrid (2018-T2/TIC-10494), the International Research Agenda Programme AstroCeNT (MAB/2018/7) funded by the Foundation for Polish Science (FNP) from the European Regional Development Fund, and the European Union's Horizon 2020 research and innovation program under grant agreement No 952480 (DarkWave). Studentship support from the Rutherford Appleton Laboratory Particle Physics Division, STFC and SEPNet PhD is acknowledged. We thank SNOLAB and its staff for support through underground space, logistical, and technical services. SNOLAB operations are supported by the CFI and Province of Ontario MRI, with underground access provided by Vale at the Creighton mine site. We thank Vale for their continuing support, including the work of shipping the acrylic vessel underground. We gratefully acknowledge the support of the Digital Research Alliance of Canada, Calcul Québec, the Centre for Advanced Computing at Queen's University, and the Computational Centre for Particle and Astrophysics (C2PAP) at the Leibniz Supercomputer Centre (LRZ) for providing the computing resources required to undertake this work.

*Speaker

1. The DEAP-3600 experiment instrumentation

The DEAP experiment, located at SNOLAB in Sudbury, Canada, aims to detect dark matter by observing nuclear recoil signals from interactions between weakly interacting massive particles (WIMPs) and argon nuclei. The detector consists of a large volume of liquid argon (LAr) contained within an acrylic vessel (AV) that is surrounded by light guides and photomultiplier tubes (PMTs) for light detection. The entire setup is submerged in a water-filled cylindrical tank called the muon veto (MV) for additional shielding and background rejection [1]. Pulse shape discrimination (PSD) is used to distinguish between electronic-recoil (ER) and nuclear-recoil (NR) signals in the WIMP search region [2].

The experiment uses a total of (3269 ± 24) kg of liquid argon distilled from the atmosphere [3]. The detector is partially filled to approximately 55 cm above the equator with LAr and the remaining volume is occupied by gas argon (GAr). The inner layer of the acrylic vessel is coated with a tetraphenyl butadiene (TPB) layer to shift the scintillation light from 128 nm to a visible spectrum peaking at 420 nm. This light is captured by 255 photomultiplier tubes (PMTs) which point inward and are optically coupled to the AV by acrylic 45 cm-long light guides. The AV and PMTs are enclosed in a stainless steel shell which is constantly flushed with radon-scrubbed nitrogen gas. To reduce the volume of data coming from ^{39}Ar decays, a prescale region defined with low F_{prompt} between 50-564 keV registers only one event every 100. Timestamps and total charge of these prescaled events are however recorded.

The muon veto of the DEAP experiment consists of a steel cylinder filled with ultrapure water. The cylinder has a height of 779 cm and a diameter of 780 cm. The interior of the cylinder is equipped with 48 Hamamatsu R1408 8" PMTs, which are mounted on the steel shell facing outward towards the water volume. This configuration maximizes the light collection efficiency while minimizing the amount of material needed for the PMT mounting. A vinyl liner made of PVC #328 covers the inside of the water tank, serving as a white diffuse reflector to enhance the light collection. To maintain high purity, the ultrapure water is continuously purified using a purification system loop. The temperature of the MV is kept constant at around 284 K to ensure the stability of the PMT gains and dark rates, and it is continuously monitored using a distributed control system. For details about the data acquisition system or the detector, please refer to [1].

The second data collection campaign ran from November 4, 2016 to March 28, 2020. Analysis of data collected until October 31, 2017 found no evidence for signal in the search for WIMPs [4]. Upcoming results will present the search for WIMPs over the whole dataset.

2. Pulse-shape discrimination

The DEAP-3600 experiment utilizes liquid argon to effectively discriminate between ER background events and NR events from α particles, neutrons, and potential WIMP signal. This is possible because argon exhibits two distinct scintillation lifetimes: the singlet state, decaying rapidly within a few nanoseconds, and the triplet state, decaying over a longer period of approximately 1.4 μs [5]. Electron recoil events, resulting from interactions like β , γ , and muon interactions, predominantly excite the triplet state, leading to scintillation light emission lasting on the order of microseconds. On the other hand, interactions involving α particles, neutrons, or WIMPs predominantly populate

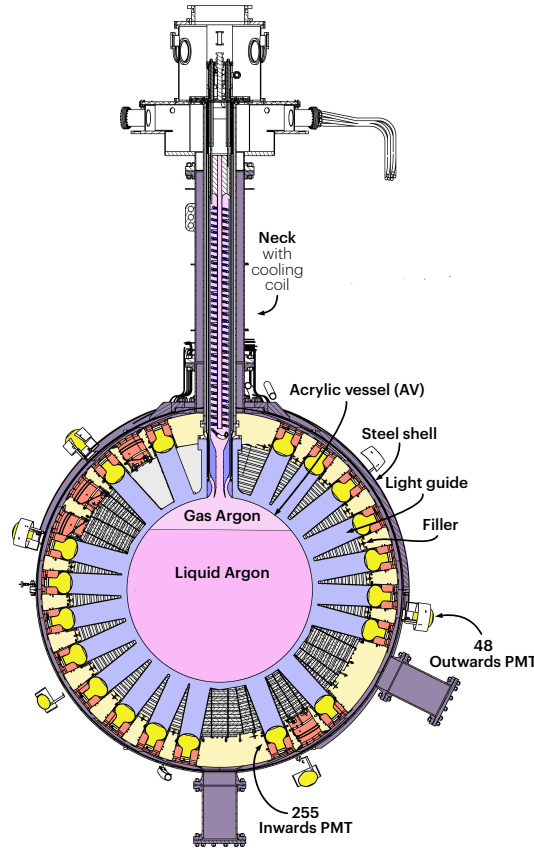


Figure 1: Cross-section drawing of the DEAP-3600 detector located inside the muon veto detector (not shown).

the singlet state. The F_{prompt} parameter, defined in Equation (1), is employed to characterize events, where higher values indicate events exhibiting prompt light emission, thus identified as NR. Pulse shape discrimination (PSD) plays an important role in the success of the experiment.

$$F_{\text{prompt}} = \frac{\int_{-28\text{ns}}^{150\text{ns}} PE(t)dt}{\int_{-28\text{ns}}^{1.6\mu\text{s}} PE(t)dt} \quad (1)$$

Figure 2 depicts the effectiveness of PSD in distinguishing between ER and NR events: two distinct distributions can be seen. At about 18 keVee, a nuclear recoil acceptance of 50% with a leakage probability of about 10^{-10} is reached with the nSc-based algorithm. Indeed, DEAP uses two different methods to calculate the number of photons. The first one calculates the integral of the pulse and divides it by the mean of a single photo-electron charge (SPE). This way of calculating the charge is, however, biased due to the PMTs afterpulsing which happens in about 10% of the waveforms. The second method, the so-called nSC-based algorithm, uses a likelihood function, based on Bayes' theorem, which estimates the number of photo-electron according to the pulse charge, the LAr scintillation probability density function (PDF), the times of preceding pulses, the afterpulse time and charge PDF, and the SPE charge distribution of the PMT. Further information

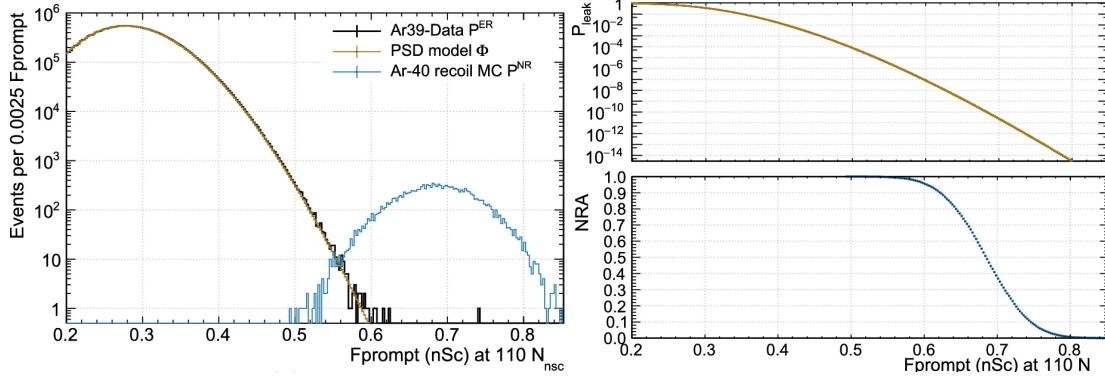


Figure 2: The distributions of F_{prompt} (nSc-based) at $110 N_{\text{nsc}}$ are presented for ^{39}Ar beta decay events along with the model fit and for simulated ^{40}Ar NR events. Taken from [2]

regarding the PSD technique and a comparison of leakage probabilities among four different PSD estimators can be found in [2].

3. ^{39}Ar specific activity

Atmospheric argon predominantly consists of the stable isotope ^{40}Ar but it also contains traces of the isotope ^{39}Ar which was activated by cosmic rays. The ^{39}Ar isotope undergoes a unique first-forbidden β decay with a half-life ($T_{1/2}$) of (269 ± 9) years [6] and a Q-value of (565 ± 5) keV [7]. ^{39}Ar decays constitute the main background of the experiment but are well constrained by the PSD method explained in the previous section. This background can nonetheless be used to measure the specific activity of the β decay of ^{39}Ar using the scintillation signals produced by the decay of this isotope within the detector.

In this analysis, the PSD parameter is used to capture only events originating from ^{39}Ar . Afterward, the specific activity is calculated by estimating the total number of ^{39}Ar decays (N) within a given live time (T_{live}) and mass (m_{LAR}), as defined by the equation:

$$S_{\text{Ar}39} = \frac{N}{T_{\text{live}} \cdot m_{\text{LAR}}} \quad (2)$$

The live time is corrected for the detector's read-out dead time and for the cuts applied. The number of single ^{39}Ar decays is calculated by fitting a model composed of single decays, double decays, and other electronic recoil backgrounds to the data. An example of the fit is shown in the left plot of Figure 3. The number of single decays is then determined by the integral of the single decay fit times the prescale factor divided by the bin size and an efficiency factor (ϵ). The efficiency is meticulously calculated through a data-driven approach and compared to Monte Carlo simulations.

Pile-up events involving ^{39}Ar , either with other electronic recoil backgrounds or nuclear recoils, are considered. The double ^{39}Ar pile-up events are accounted for using a spectral fit, while the others are derived through a first-order approximation. The number of ^{39}Ar decays in pile-up events is then added to the number of single-decay events to obtain N .

Using 167 live days of data, the specific activity of ^{39}Ar at the time of atmospheric extraction is measured to be $(0.964 \pm 0.001_{\text{stat}} \pm 0.024_{\text{sys}})$ Bq/kg $_{\text{atmAr}}$, taking in account the correction for the

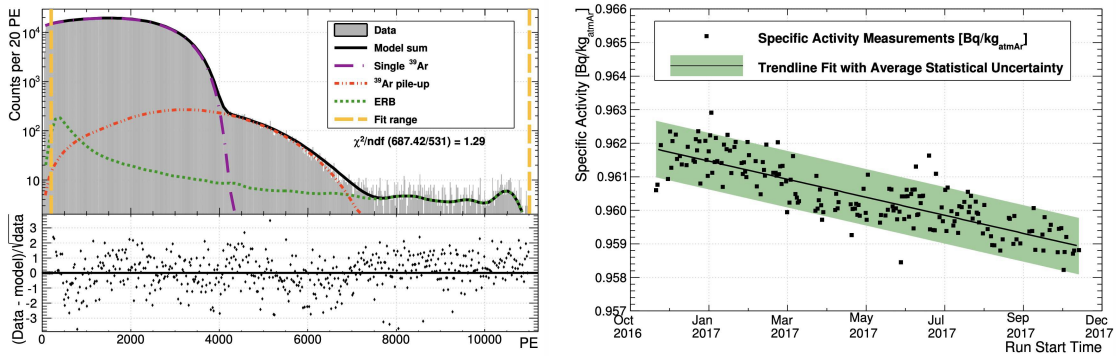


Figure 3: Right: illustration of an instance of the fit performed on one run, with the color lines illustrating the implemented models. The bottom panel displays the residual between the fit function and the corresponding data. The run in question spans approximately 28.5 hours. Left: the measured specific activity of ^{39}Ar plotted against the run time for the complete dataset. The exponential trendline fit is depicted, accompanied by an error band representing the average statistical uncertainty. Note that the systematic uncertainty band extends beyond the y-axis range depicted in this figure. Taken from [3].

time between the extraction of argon from the atmosphere and the running time of the detector. The specific activity of ^{39}Ar during the operation of DEAP-3600 is shown on the right plot of Figure 3. This measurement is consistent with results from other experiments [8, 9] and represents a leading level of precision. Further details can be found in [3].

4. Planck scale dark matter

In the search for Planck-scale mass dark matter, a multiple-scatter technique is employed which involves identifying multi-scattering events that could be caused by dark matter particles with extremely large masses up to the Planck scale ($\approx 10^{19}$ GeV/c²). These particles would produce distinct signatures which are typically excluded in traditional WIMP searches.

The analysis is built in a blind fashion using simulations. Dark matter is simulated 80 km above the Earth’s surface and propagated to the detector while assuming continuous energy loss throughout its trajectory. The simulations use a Standard Halo Model (SHM) velocity distribution. A multiple peaks finding algorithm is utilized to estimate the number of peaks in the summed waveforms of all the PMTs. Unlike WIMP searches which focus on high F_{prompt} values, multiple scattering events can result in lower F_{prompt} values, particularly for higher levels of detected photoelectrons i.e. higher energies.

The data are divided into four distinct regions, each corresponding to different waveform behavior and dominant background criteria. The left plot of Figure 4 illustrates the dependence of F_{prompt} on increasing values of measured photoelectrons and cross-sections, with different colors representing the four defined search regions.

Using about 813 live days of data, the background expectation across all defined regions was found to be (0.05 ± 0.03) events. Upon unblinding the data, no event was observed in any of the signal regions, resulting in an exclusion of all models predicting more than 2.3 events with a 90% confidence level.

These results were interpreted within two models, allowing DEAP to constrain the mass-cross-section phase space of dark matter search. Model I assumes dark matter to be opaque to nuclei,

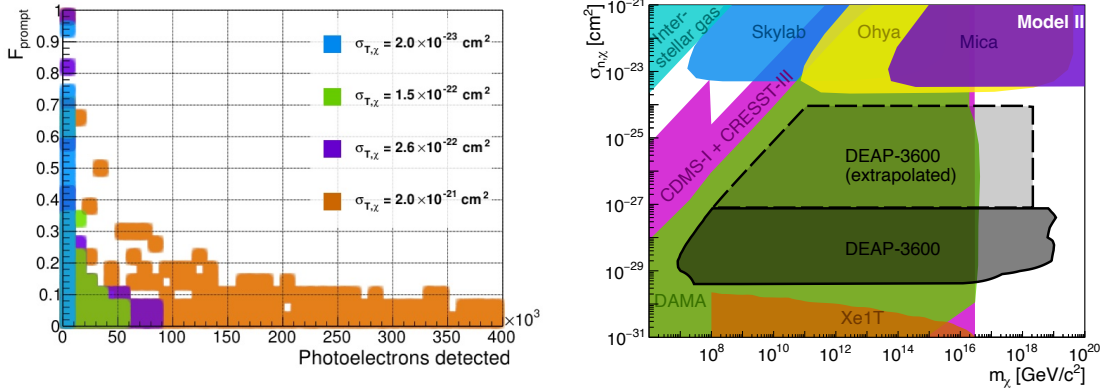


Figure 4: Left: The dependence of F_{prompt} on increasing photoelectron (energy) and increasing cross-section, with different colors representing defined search regions. Right: Constraints on the mass-cross-section phase space of dark matter search within two models. Taken from [10].

with the momentum transfer solely determined by the geometric size of the dark matter particle regardless of the target nucleus. Model II applies a scaling of the cross-section proportional to A^4 , where A represents the target mass number. This scaling is commonly used and the corresponding constraints are shown in the right plot of Figure 4. Constraints from the Model I as well as further details on the methodology can be found in [10].

5. Non-relativistic effective field theory and halo substructure interpretation

The results presented in [4] were reinterpreted in the context of non-relativistic effective field theory (NREFT) while considering the presence of kinematically distinct halo substructures in dark matter, assuming that DM substructures would exhibit similarities to the observed stellar substructure. The NREFT provides a parameterization of possible dark matter-nucleon interactions using operators [11], here the analysis focuses on operators O_1 , O_3 , O_5 , O_8 , and O_{11} . Where O_1 represents the standard isoscalar interaction, while O_3 couples with the spin of the nucleon, and O_5 , O_8 , and O_{11} couple with the dark matter's spin and exhibit dependence on the variables (q, v_\perp) , (v_\perp) , and (q) respectively.

The results of the analysis are reported in terms of cross-section limits. The study also explores scenarios where the dark matter is either an isoscalar (IS), an isovector (IV), or xenophobic (XP), leading to a stronger exclusion space from DEAP-3600 compared to XENON1T. This emphasizes the importance of using detectors with different nuclei to explore a wider range of dark matter models. The left plot in Figure 5 illustrates the different exclusion limits for the various operators and dark matter models.

The analysis takes into account various substructures, including streams, debris flow, and in-falling clumps, such as the Gaia Sausage, Nyx stream, and Helmi stream. These substructures can exhibit velocity distributions prograde, perpendicular, or retrograde to the laboratory rest frame. Based on estimates for the stellar substructure fraction, the analysis assumes that dark matter substructures could range from 0% to 30%, except for the Gaia Sausage substructure, where a scenario of 0% to 70% range is considered. The right plot in Figure 5 displays the upper limits on O_1 from the potential substructures. As expected, the substructure with a flow anti-parallel

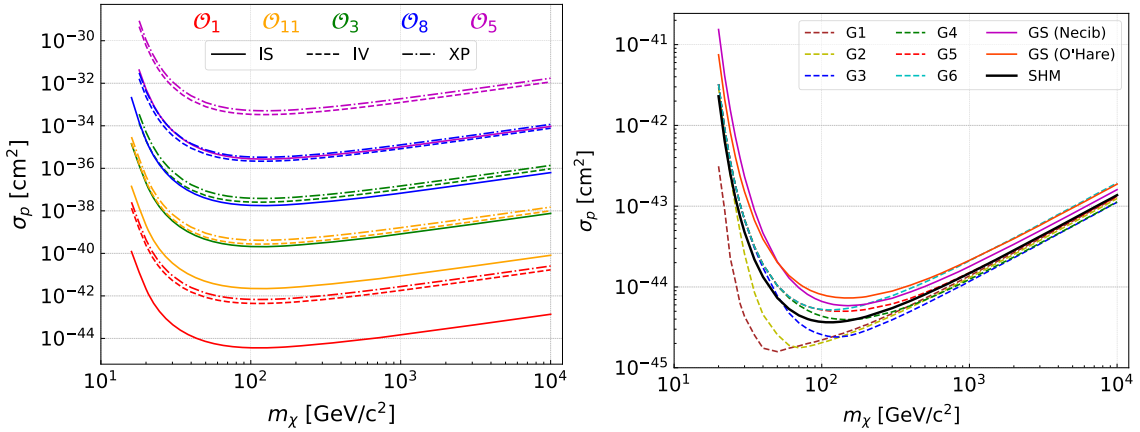


Figure 5: Left: Exclusion limits for different operators and dark matter models. Right: Upper limits on \mathcal{O}_1 from the potential DM substructures. Taken from [12].

to the laboratory rest frame increases the constraints and oppositely, the parallel ones loosen the constraints.

This very detailed analysis explores multiple scenarios and draws exclusion lines for the different operators under study. For more precise details on the models, interactions, formulas, and exclusion curves, please refer to [12].

6. Hardware Upgrade

The hardware upgrade for the DEAP-3600 detector involves several key improvements. Firstly, the introduction of pyrene-coated flow guides will enable the rejection of scintillation light induced by alphas from ^{210}Po in the neck of the detector. This enhancement will allow for better discrimination of signal events. Additionally, an external cooling system will be installed to prevent argon condensation on the flow guides, ensuring stable and reliable operation of the detector.

The analysis of DEAP-3600 data revealed an overabundance in the α -decay background, which is found to be consistent with α -decay within a small number of dust particulates ranging from $1\ \mu\text{m}$ to $50\ \mu\text{m}$ in diameter in the liquid argon, as shown in Figure 6. To mitigate the impact of dust background, a new extraction and filtration system for the liquid argon will be implemented to remove dust particles in the detector. The objective is to enhance the overall performance and sensitivity of the DEAP-3600 detector.

7. Conclusion

In conclusion, the DEAP-3600 experiment has achieved significant milestones in the field of dark matter detection. It has already set the most stringent exclusion limit for high-mass WIMPs in liquid argon, showcasing its ability of effective pulse shape discrimination. The re-analysis of WIMP results with non-relativistic effective field theory (NREFT) and non-standard galactic halo models has provided valuable insights for DM exclusion limits. Tuning the detector to heavy, multi-scattering dark matter candidates extends world-leading exclusion limits up to Planck scale masses. Precise measurements of atmospheric argon's specific activity have contributed to our understanding of this background source. Ongoing efforts include upcoming analyses of WIMPs

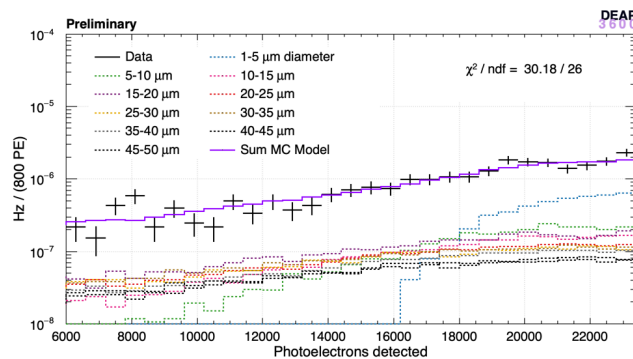


Figure 6: The plot shows the particulate sizes and the amounts necessary for dust alpha decays to accurately describe the observed data. The fit of all particulates is shown in purple compared to the data shown in black. candidates with a profile likelihood ratio analysis over the full dataset collected so far, a muon flux measurement using the muon veto detector, and a search for ^8B solar neutrinos scattering in argon. Finally, detector upgrades are also underway, enhancing the capabilities of the experiment.

References

- [1] DEAP Collaboration, P. A. Amaudruz *et al.*, *Astropart. Phys.* **108** (2019) 1–23.
- [2] DEAP Collaboration, P. Adhikari *et al.*, *Eur. Phys. J. C* **81** no. 9, (2021) 823.
- [3] DEAP Collaboration, P. Adhikari *et al.*, “Precision measurement of the specific activity of ^{39}Ar in atmospheric argon with the deap-3600 detector,” 2023. [arXiv:2302.14639](https://arxiv.org/abs/2302.14639) [[physics.ins-det](https://arxiv.org/abs/2302.14639)].
- [4] DEAP Collaboration, R. Ajaj *et al.*, *Phys. Rev. D* **100** no. 2, (2019) 022004.
- [5] DEAP Collaboration, P. Adhikari *et al.*, *Eur. Phys. J. C* **80** no. 4, (2020) 303.
- [6] R. Stoenner, O. Schaeffer, and S. Katcoff, *Science* **148** no. 3675, (1965) 1325–1328.
- [7] M. Wang, G. Audi, A. H. Wapstra, F. G. Kondev, M. MacCormick, X. Xu, and B. Pfeiffer, *Chin. Phys. C* **36** no. 12, (2012) 1603–2014.
- [8] WARP Collaboration, P. Benetti *et al.*, *Nuclear Instruments and Methods in Physics Research Section A: Accelerators, Spectrometers, Detectors and Associated Equipment* **574** no. 1, (2007) 83–88.
- [9] ArDM Collaboration, J. Calvo *et al.*, *Journal of Cosmology and Astroparticle Physics* **2018** no. 12, (2018) 011.
- [10] DEAP Collaboration, P. Adhikari *et al.*, *Phys. Rev. Lett.* **128** no. 1, (2022) 011801.
- [11] A. L. Fitzpatrick, W. Haxton, E. Katz, N. Lubbers, and Y. Xu, *Journal of Cosmology and Astroparticle Physics* **2013** no. 02, (Feb, 2013) 004.
- [12] DEAP Collaboration, P. Adhikari *et al.*, *Phys. Rev. D* **102** no. 8, (2020) 082001. [Erratum: *Phys.Rev.D* 105, 029901 (2022)].